LAWRENCE
LIVERMORE
NATIONAL
LABORATORY

UCRL-JRNL-230783

ESTIMATING THE STRENGTH OF SINGLE-ENDED DISLOCATION SOURCES IN MICROMETER-SIZED SINGLE CRYSTALS

S. I. Rao, D. M. Dimiduk, M. Tang, T. A. Parthasarathy, M. D. Uchic, C. Woodward

May 8, 2007

Philosophical Magazine

ESTIMATING THE STRENGTH OF SINGLE-ENDED DISLOCATION SOURCES IN MICROMETER-SIZED SINGLE CRYSTALS

S.I. Rao*, D.M. Dimiduk, M. Tang#, T.A. Parthasarathy*,
M.D. Uchic and C. Woodward^

Air Force Research Laboratory, Materials and Manufacturing Directorate,
AFRL/MLLM Wright-Patterson AFB, OH 45433-7817

*UES, Inc., 4401 Dayton-Xenia Rd, Dayton, OH 45432-1894

#Lawrence Livermore National Laboratory, P.O. Box 808, L-45 Livermore, CA 94551

^Northwestern University, Department of Materials Science and Engineering, 2220 Campus Drive, Evanston, IL 60208-3108

ABSTRACT

A recent study indicated that the behavior of single-ended dislocation sources contributes to the flow strength of micrometer-scale crystals. In this study 3D discrete dislocation dynamics simulations of micrometer-sized volumes are used to calculate the effects of anisotropy of dislocation line tension (increasing Poisson's ratio, υ) on the strength of single-ended dislocation sources and, to compare them with the strength of double-ended sources of equal length. This is done by directly modeling their plastic response within a 1 micron cubed FCC Ni single crystal using DDS. In general, double-ended sources are stronger than single-ended sources of an equal length and exhibit no significant effects from truncating the long-range elastic fields at this scale. The double-ended source strength increases with Poisson ratio (υ), exhibiting an increase of about 50% at $\upsilon = 0.38$ (value for Ni) as compared to the value at $\upsilon = 0$. Independent of dislocation line direction, for υ greater than 0.20, the strengths of single-ended sources depend upon the sense of the stress applied. The value for α, in the expression for

strength, $\tau = \alpha(L)\mu b/L$ is shown to vary from 0.4 to 0.84 depending upon the character of the dislocation and the direction of operation of the source at ν corresponding to that of Ni, 0.38 and a length of 933b. By varying the lengths of the sources from 933b to 233b, it was shown that the scaling of the strength of single-ended and double-ended sources with their length both follow a $\ln(L/b)/(L/b)$ dependence. Surface image stresses are shown to have little effect on the critical stress of single-ended sources at a length of ~250b or greater. The relationship between these findings and a recent statistical model for the hardening of small volumes is also discussed.

1.0 INTRODUCTION

Recent experimental studies discovered that the proximity of free surfaces bounding small volumes at the micrometer scale produces strong size-affected strengthening in face-center cubic (FCC) single crystals, even for high initial dislocation densities [1-8]. In an unpublished study [9], the present authors used large scale 3D dislocation dynamics simulations (DDS) to explicitly model the deformation behavior of micrometer-sized crystals. In that work two underlying mechanisms that give rise to free-surface size effects were identified. One mechanism—surface-mediated source hardening—was identified as being especially potent in micrometer-scale volumes. This effect arises from the conversion of pre-existing double-ended dislocation sources into single-ended sources that intersect and interact with free surfaces. Such a conversion establishes a new characteristic length for the dislocation sources. The sources were shown to adopt configurations that are related to those previously described for small constrained volumes by Blankenhagen, et. al., [10] but with a key difference being that the

dislocation lines are truncated by intersecting the free surfaces. In samples below a critical size, the truncation of dislocation sources, together with the under-sampling of an assumed initially random distribution of dislocation sources, leads to smaller average source lengths when compared to a bulk sample of equal dislocation density. This surface-mediated source-hardening contribution was analytically modeled and shown to account for a significant portion of the strengthening observed in FCC micrometer sized crystals [11]. However, for those calculations, the dislocation line tensions were taken to be isotropic and the strength of single-ended dislocation sources of a length 'L' was assumed to be $\alpha\mu b/L$, where α is of the order of 1, μ is the shear modulus and 'L' is the length of the single-ended source [11]. Further, those findings were based upon 3D DDS results that used a simplifying assumption for the behavior of the dislocations that intersected the surfaces of the simulation cell. That assumption was necessary for efficient parallel computation of large simulation cells having free surfaces rather than periodic boundary conditions (a representation of deforming microcrystals). Thus, the question remains open as to the actual source strengths that may be expected for small volumes that contain principally single-armed sources that intersect a surface. An initial examination of that question is taken up by the present study.

Previously, the strengths of single-ended and double-ended sources were modeled using isotropic elastic theory, at a value of Poisson's ratio of 0.333 [12]. These strengths have been evaluated for the special case of a glide plane intersecting the surface at right angles in a semi-infinite-half-space material. As a result, a simple image construction was possible for that analysis to include the influence image forces on source strength. The study shows that the strengths of single-ended sources are dependent upon the

direction of traverse of the source and are weaker than those of double-ended sources by a factor of 1.3 - 2.6 [12]. That study also showed that the scaling of the strength of both single-ended and double-ended sources with their length follows a ln(L/b)/(L/b) dependence. However, within a current broader context, it is desirable to separate the influence of the image stress from the overall behavior of the dislocation sources and to understand the behavior of such sources for more general dislocation configurations. Such a separation is motivated by the fact that is not yet possible to impose accurate treatments of the image forces within large-scale parallel computing codes that are a must for many 3D DDS studies, including the study of microcrystal flow.

Accordingly, in this work a DDS technique is used to calculate the effects of anisotropy of dislocation line tension (within the isotropic elasticity assumption) on the strengths of single-ended sources and, to compare them with the strengths of double-ended sources of equal length. This is done by directly modeling their plastic response within a 1 micron cubed FCC Ni single crystal using DDS where the glide plane intersects the surface at a crystallographically-appropriate angle of 54.7^{o}. A comparison of simulation results with an accurate consideration of image stresses, here called Full Free Surface Treatment (FFST), with similar results that did not include consideration of image stresses, here called Simplified Surface Approximation (SSA) is performed. Both of these categories of results are in turn compared with the previous results on strengths of single-ended sources by Pichaud et. al., [12]. The implications of these results are discussed.

2.0 SIMULATION TECHNIQUE

A version of the 3-dimensional parallel DDS code "ParaDiS," [13,14] developed at Lawrence Livermore National Laboratory, was used to simulate the stress-strain response of single-ended and double-ended sources in a 1 micron cubic crystal. In ParaDiS, dislocation lines are represented as a series of nodal points connected by straight-line segments. The glide-plane force on each node is calculated using isotropic linear elasticity and the velocity of a node is taken to be linearly proportional to the force according to a viscous damping law. In these simulations, the velocity was set at 4000 b/s for a force due to an applied shear stress of 1 Pa, where b is the magnitude of the Burgers vector of the gliding dislocation (0.25 nm). For these simulations the shear modulus and Poisson's ratio were set to values of 59.9 GPa and 0.379, respectively. These values correspond to the shear modulus $= \mu_{111}$ for Ni and Poisson's ratio, $\upsilon = c_{12}/(c_{11}+c_{12})$, where c_{11} and c_{12} are the cubic single-crystal elastic constants of Ni [15]. To describe anisotropic elasticity effects correctly in the isotropic approximation for double-ended sources, Scattergood and Bacon [16] suggest using an isotropic shear modulus as $\mu = 4\pi E_{screw}/b^2$ and, Poisson's ratio, υ, as $1\text{-}E_{screw}/E_{edge}$, where E_{screw} and E_{edge} are the pre-logarithmic line energy factors for infinite straight a/2<110> screw and edge dislocations on the {111} plane in FCC Ni. Such calculations give $\mu = 78.7$ GPa and $\upsilon = 0.38$ for Ni. Therefore, critical stresses given in this manuscript for single-ended and double-ended sources at a Poisson's ratio of 0.38, must be scaled to a shear modulus of 78.7 GPa from a shear modulus of 59.9 GPa, to obtain their absolute values in Ni.

For the simulations, a constant strain rate of 50 s^{-1} was imposed along the [41-3] crystal direction. The (1-1-1)[110] slip system is maximally stressed under these conditions, having a Schmidt factor of 0.47. Both the single-ended and double-ended sources in the simulation were made to lie on this slip system. If at any time step, the specimen plastic displacement rate was lower than the applied rate, the applied stress was incremented to obey a constant applied displacement rate. However, if the specimen plastic displacement rate was higher than that of the programmed rate, the applied stress was kept constant, thus permitting source expansion. Increments in stress occurred only after it was determined that the total displacement at a particular time was less than the applied displacement rate multiplied by the elapsed time.

The ParaDiS code was modified in the following manner to qualitatively account for dislocation surface effects (the SSA). An approximation to the dislocation-surface interaction effects is useful because including the details of image effects in large-scale parallel DDS of dislocation ensembles evolving over significant strains is computationally challenging. This is particularly true for the range of simulation cell sizes required to describe the size scaling effects observed in recent micro-compression experiments in FCC metals; a range from 0.2 – 20μm diameter [1-8]. Within calculations using this approximation, dislocation segments that expand to reach the surface (those that would be lying on the surfaces) are deleted as though they exited the glide plane of the dislocation source. Within the SSA method, the velocity of the terminal dislocation nodes at the surfaces (surface nodes) was modified such that the velocity components perpendicular to both the free surface and the glide plane were zero, thus causing the node to track the surface trace of the slip plane. As described in Section 4 we found that

this treatment, SSA, not only qualitatively captures the most important free surface effect of establishing a new critical source length for flow, but is also computationally efficient within a parallel environment. Separate simulations using a serial version of ParaDiS were used to show that small changes in the strength of single armed sources can be expected due to the influence of the image forces acting on dislocations from free surfaces (our FFST method). Selected source configurations acting under the influence of image forces were examined to quantify these effects. The image stresses were modeled using a hybrid technique where the singular and non-singular parts of the image stresses are dealt with separately [17]. The analytic solution for a semi-infinite straight dislocation intersecting the surface of elastic half-space is used to account for the singular part of the image stress, while the remaining non-singular part is treated using the standard finite-element method [17]. As described in Section 4, the effect of the image force acting on a single-arm source was found to decrease the source strength by less than ~10% when compared with the SSA method. Comparison of the dislocation configuration at the critical point shows that the dislocation is slightly longer in the case where image stresses are included. Thus, the image forces were neglected for the majority of this study.

3.0 SOURCES WITHIN THE SIMPLIFIED SURFACE APPROXIMATION

One objective for this work was to determine the effect of line energy anisotropy on the strength of the single-ended and double-ended dislocation sources in small material volumes. Consequently, four types of simulations were conducted; i) double-ended sources under both isotropic and anisotropic line energy, ii) single-ended sources under

both isotropic and anisotropic line energy, iii) single-ended sources of varying line orientation acting under anisotropic line energy and finally, iv) single-ended and double-ended sources of varying line length under anisotropic line energy. For the first case analytical results exist in the literature for the equivalent configuration acting within an infinite volume and these are used for comparison. The infinite-volume case has also been extended to include an expression for the effect of Poisson's ratio on the double-ended source strength based on prior simulation studies. In the isotropic limit, the strength of a single-armed source is expected to be half that of a double-ended source of the same length. These prior results were verified for a small volume and then the effects of dislocation line energy anisotropy and line character on both double-ended and single-ended sources are examined. Three dislocation characters, edge, screw and 30^o mixed dislocation characters were considered.

3.1 Double-ended Sources in a Small Volume

The source strengths for double-ended sources in small crystals were calculated using sources of length 933b, placed at the center of a cube of material, whose sides were 1 micron in length. The source length was determined by introducing a random-length Frank-Read source and allowing it to expand and intersect the free surface. Thus, the source length was about one-fourth of the cube-edge length. The effect of Poisson's ratio on double-ended sources was calculated using a 30^o mixed-character dislocation. The results for the strength of double-ended sources as a function of Poisson's ratio are shown in Fig. 1. For the double-ended sources in an infinite medium, the critical stress as a function of Poisson's ratio can be written as [16]

$$\tau(\upsilon) = \frac{\alpha\mu b}{L} = \frac{\mu b}{L} C\left(\frac{3}{4(1-\upsilon)} + \frac{1}{4}\right) \quad (1)$$

A fit of equation 1 to the simulated critical stress data for double-ended sources is shown in Fig. 1 and the correspondence is very good for a value of C = 0.823. Thus, the influence of the finite volume is negligible at the 1 micrometer scale and above.

3.2 Single-ended Sources in a Small Volume

Critical stresses were evaluated for the single-ended sources as a function of Poisson's ratio, keeping the source length at 933b. The results are shown in Fig. 2, for the case of a source whose initial configuration was a straight line extending from a fixed node inside the cube to the surface and the line character being a 30^o mixed dislocation. The strength of such a source depended upon the sign of the applied stress which resulted in the operation of the source in the 'forward' or 'reverse' direction. The results are shown in comparison to the double-ended source results, for both the forward and reverse motion of the dislocation. As shown by Fig. 2, one may observe that for the case of isotropic line tension (υ = 0-0.1), the source strength of a single-armed dislocation source is nearly half that of the equivalent double-ended source. This result is in agreement with published estimates of the critical stress for single-ended sources in a line energy isotropic material [18]. Further there is no significant difference between the forward and reverse directions.

However, for the anisotropic line energy case (υ >0), Fig. 2 shows that for the forward direction, the critical stresses increase rapidly with increasing Poisson's ratio (similar to those for double-ended sources). However, for the reverse direction, the

source strengths increase more gradually. The critical stresses for single-ended sources are more than half of those for double-ended sources when stresses act in the forward direction and, less than half when stresses act in the reverse direction, when the Poisson's ratio is large (>0.3). These results are similar to the simulation results of Pichaud, et. al., [12] at a Poisson's ratio of 0.333. Note that for all of the FCC microcrystals used in experimental studies reported in the literature, viz., Cu, Ni, Au and Al [1-8], Poisson's ratio is relatively large (>0.3) and the anisotropy in critical stress between the forward and reverse directions for the 30^o degree single-ended source is expected to occur. This result suggests that there is an intrinsic scatter to the source strengths even for fixed source lengths.

3.3 Origin of Source Strength Asymmetry

For the small volumes examined here, the stress-strain curves and dislocation configurations at the critical stress offer insights into the nature of the source-strength asymmetry with respect to the direction of operation. Consider a single-ended source of length 933b, inserted into a one micron cubic simulation cell, residing on a {111} plane and having its fixed point inside the cell and the other end on the {100} surface. For this case being a 30^o mixed-character dislocation line source, the source has a line direction <211> which is 30^o away from the <110> screw-line direction and perpendicular to the surface edge trace, a <01-1> direction. Figure 3 shows the stress-strain response of such a source (30^o forward) along with two other sources (30^o reverse and screw character). The stress-versus-strain response was purely elastic-plastic with a critical stress of 114 MPa (CRSS of 54.5 MPa in Fig. 2). At the critical stress, the single ended-source

traverses the (1-1-1) glide plane continuously leading to uninhibited plastic deformation. The stress-strain response of the screw-character dislocation source was also purely elastic-plastic with a critical stress of 90 MPa (CRSS of 42.3 MPa in Fig. 2). In this case, the Burgers vector of the initial source was chosen, for convenience, to be a <211> direction such that the initial source had a screw-character direction. For the third curve (30^o reverse), the input Burgers vector (1/2<110>) was reversed as compared to 30^o forward, such that the source moves in the opposite direction as compared to 30^o forward under the applied stress. In this case, the stress-strain curve shows a small strain burst at 57 MPa (CRSS of 27.2 MPa in Fig. 2) before uninhibited plastic deformation at 64 MPa (CRSS of 30.6 MPa in Fig. 2).

Figure 4 shows the initial (stress free) and critical configuration (maximum stress) of these dislocations. The results show that at the very beginning of the simulation, when the applied stress is almost zero, the source rotates from the 30^o character to the screw-character position, a <110> direction (for both the 30^o forward and 30^o reverse case). This occurs because of the lower line-energy per-unit-length for the screw-character dislocation. It is known in the literature that the most frequently observed surface effect for dislocations is Lothe's force which causes dislocations to rotate to lower their line energy [19]. Thus, the energy increase due to the necessary line length increase as it rotates is more than offset by the energy decrease due to line direction change, from 30^o to zero degrees. For the screw-character source case, no rotation takes place since the initial line direction itself is a low-energy line direction. The critical configurations for these sources are shown in Fig. 4. Note that the line tension forces tend to curve the sources about the fixed point and the screw-character direction. The direction of traverse

for the single-ended source acting in the 30^o forward case is such that the source is curving initially in a direction with decreasing line length (back toward the original 30^o direction). However, for the 30^o reverse case, the source is curving in a direction with increasing line length, away from the original 30^o position. Therefore, the asymmetry in the critical stress between the forward (moving back toward 30^o position) and reverse (moving away from 30^o position) directions of motion is most probably related to line tension forces. These forces make it easier for the source to curve in a direction with increasing line length as compared to a direction with decreasing line length. For the screw-character case, the source is curving about the fixed point and the initial direction, which has a line length intermediate to the previous two cases and, the corresponding critical stress of 90 MPa lies between 114 MPa (30^o forward) and 57 MPa (30^o reverse). For both the 30^o forward and screw-character cases, once the source overcomes the critical configuration, it continuously traverses the glide plane leading to uninhibited plastic deformation. For the 30^o reverse case, once the source overcomes the critical configuration shown in Fig. 4, it traverses the glide plane and reaches another critical configuration on the opposite surface edge, which corresponds to (in our nomenclature) a 30^o forward source for the opposite surface edge, with a larger length. For this source this position is overcome at a stress of 64 MPa and thereafter, the source continuously traverses the glide plane.

The critical stress results suggest that for a Poisson's ratio of 0.38 (i.e. Ni), the 30^o single-ended source has strengths of approximately 0.8μb/L in the forward direction and

0.4μb/L in the reverse direction, while double-ended sources are stronger than the corresponding single-ended sources.

4.0 EFFECT OF IMAGE STRESSES USING THE FFST

In the previous section, calculations of the plastic response of single-ended sources of length 933b in a 1 micron cubic cell were presented. For those simulations the image stresses that make the surface traction-free were not considered. For the set of simulations presented in this section, the images forces were included by the following method. A different serial version of the ParaDiS code was employed that uses a hybrid technique [17] for calculating the image stresses. The hybrid technique considers the image-stress field as a superposition of two solutions, analytic and FEM based. The analytic solution is the image-stress field of a semi-infinite straight dislocation intersecting the free surface of a semi-infinite half-space. The geometry of this dislocation is chosen such that its image stress contains the same singularity as the image stress of the dislocation of interest. The second, FEM solution, is the difference between these two image stress fields; by construction it is a non-singular function of space and converges much faster than a direct FEM calculation of the complete image-stress field [17, 20].

When image stresses are also considered for the simulation cell, there are minor differences in the exact configurations and critical stresses adopted by dislocation sources. For example, the 30^o single-ended source does not rotate all the way to the screw-character line position as was seen in the earlier SSA-method calculations. Rather,

that source rotates to a position 10-15^{o} away from the screw-character position (see Fig. 5). With image forces imposed, the source tries to lie orthogonal to the cell surface [12], but these forces are resisted by line tension forces that push the line toward the screw-character position. Thus, the balancing of these two forces results in an initial position which is in between the initial 30^{o} position and the screw-character position and thereby a slightly altered source length. Under continued increase in stress, the source then bows around this initial configuration and the fixed point to attain the critical configuration at a stress of 104 MPa (CRSS of 49.7 MPa in Fig. 2). The final distance to the surface at the critical configuration is slightly larger as compared to the SSA-method case, resulting in a slight decrease of the critical stress (~10%). For the 30^{o} reverse case, the critical stress with the FFST is slightly larger, 60 MPa (CRSS of 28.7 MPa in Fig. 2), as compared to the results from the SSA method. In this case, the stress increases as a result of both the image and line energy forces tending to work against the applied stress, thus reducing the source length relative to the image-free source. Figure 6 shows similar results as are shown in Fig. 2. However, the data in Fig. 6 show the effect of sources operating under the action of image forces as a function of Poisson's ratio (using the FFST). A direct comparison of the source critical stresses between these two figures reveals that within the present image-force analysis there is only a modest effect of the image force on single-ended source strength relative to our SSA method. Overall, image stresses have only a slight effect (<~10%) on the critical stresses of single-ended sources at these sizes.

Prior studies of image-force effects reported in the literature [19] suggest that image stresses decrease rapidly as one moves away from the free surface, taking on a value of

only about 10 MPa for distance of about 50 – 100b away from the free surface. A length of 50 – 100b is equivalent to 1 or 2 nodes at or near the surface for the discretization lengths typically used in the present (and other) DDS simulations. Since the source length considered here is an order of magnitude larger than this image-stress decay distance of 50 – 100b, it is not surprising that image stresses have little effect on the critical stress of single-ended sources of length 933b. They are expected to become more significant as the source length is decreased below ~250b. In spite of these results showing a negligible influence of the image stresses, it is important to note an alternate effect that was not investigated in the present study. From prior studies, image stresses are also known to significantly increase the propensity for screw-character dislocations to cross-slip near surfaces. This occurs by the image forces acting to constrict the Shockley partials of the a/2<110> screw-character dislocation at some surfaces [19, 21, 22]. Dislocation cross-slip has not been considered in the simulation results presented here. Any cross-slip at or near the surface due to image stresses may result in a complete or partial pinning of the dislocation at the point of surface intersection, thus raising the strengths of single-ended sources toward those of a double-ended source of the same length. Thus, the present results from both the SSA and FFST methods must be viewed only as plausible lower bounds on single-ended source strengths.

5.0 LENGTH SCALING OF THE CRITICAL STRESS OF SINGLE ENDED AND DOUBLE ENDED SOURCES

Figure 7 shows a plot of the critical resolved shear stress of double-ended (30^o) and single-ended (30^o forward and 30^o backward) sources, as a function of length of the sources, with the length varying from 233 to 933b, obtained from DDS, at $\upsilon = 0.38$. Also shown in the plot are fits to the simulation data using an equation of the form

$$\tau(L) = k\mu\ln(L/b)/(L/b) \qquad (2)$$

where k is a constant. It is seen that equation (3) fits the simulation data very well, with k being 0.06 for single-ended sources (backward), 0.12 for single-ended sources (forward) and 0.18 for double-ended sources. From prior literature reports, it is well known that the critical stresses of double-ended sources scale according to equation (3) [23, 24]. Figure 7 shows that scaling according to equation (3) is also valid for single-ended sources as was observed in the simulations of Pichaud, et. al., [12] for lengths varying between $10^3 - 10^6$b. Also note that the simulations leading to Fig. 7 were performed using the SSA method. As discussed before, image stresses are expected to influence the strength of single-ended sources only when the lengths of the sources reach ~ 250b or less. Therefore, equation (2) can be considered valid for single-ended sources, for source lengths greater than 500b, as used for analysis of the Ni microcrystals [11].

6.0 SOURCE STRENGTH COEFFICIENTS FOR SINGLE ENDED AND DOUBLE ENDED SOURCES AT A POISSON'S RATIO OF 0.38

For dislocation sources, the balance between dislocation line length and line curvature leads to the following expression for the critical resolved shear stress versus source length:

$$\tau(L) = \alpha\mu b/L \quad (3)$$

where 'L' is the length of the single-ended or double-ended source. The parameter "α" is the source-strength coefficient that varies with the exact nature of the source, length of the source and the material. For these simulations, the value of Poisson's ratio was fixed at 0.38 and the values for α were determined at a length of 933b. Table 1 shows values for the coefficient for various sources that indicate a variation from 0.4 – 0.84 for single-ended sources and, 0.8 – 1.28 for double-ended sources in small volumes. Clearly, the double-ended sources are stronger than the single-ended sources. The coefficient 'α' at any length of the single-ended or double-ended sources can be obtained from their corresponding value at 933b as

$$\alpha(L) = \alpha_{933b}\ln(L/b)/6.84 \quad (4)$$

DISCUSSION & SUMMARY

To open the discussion this study is summarized as follows:

1. The strengths of single- and double-ended dislocation sources were determined for a 1 micron cubic simulation cell using a 3D DDS code and a simplified treatment of surface conditions that is amenable to efficient parallel computing. The initial length of the sources was fixed at 933b for this cell and both the line energy anisotropy (Poisson's ratio) and line character were varied.
2. Single-ended sources are weaker than the corresponding full Frank-Read sources, with the measure of strength 'α' for single ended sources varying between 0.4 – 0.84 and, for double ended sources varying between 0.86 – 1.28,

at a Poisson's ratio of 0.38. There was no observable influence from truncating an infinite volume to the 1 micrometer scale.

3. There is an asymmetry in the strength of single-ended sources depending upon the direction of traverse of the source. The direction where the distance to the surface initially decreases is stronger for Poisson's-ratio values greater than 0.2. This is in agreement with previous results from Pichaud, et. al., [12] on the strength of single-ended sources for the special case of a glide plane intersecting the surface at right angles and a Poisson's ratio of 0.333.

4. For a separate set of simulations the near-surface image force was introduced and its influence on source strength was examined for a source length of 933b to check the effect of the SSA. At these source lengths, image stresses have little effect (<10%) on the strength of single-ended sources.

5. In the absence of image stresses, the scaling of the strength of single-ended and double-ended sources with their length follows a ln(L/b)/(L/b) dependence. This is in agreement with previous results from Pichaud, et. al., [12] for source lengths ranging from $10^3 - 10^6$b.

6. Comparison of the present results on the strength of single-ended sources with previous results from Pichaud, et. al., [12] suggests that the strength of single-ended sources follows equation (2) with k given by (within 15%) [12]

$$k = 0.108 + 0.040 \cos(2\phi + \pi/3) \qquad (5)$$

where 'ϕ' is the angle between the Burger's vector and line direction of the single-ended source, for source lengths greater than 500b.

The single-ended sources envisaged here for micrometer-sized crystals are conceptually similar to the ones proposed by Blanckenhagen, et. al., [10] for the strengthening of constrained micrometer-scale volumes. Both concepts involve the setting of a new dislocation source length that is different from the initial source and governed by the presence of a constraining surface. However, there are significant quantitative differences between the constraints imposed by a grain boundary wherein the full dislocation loop is envisaged to be retained (such as in the work by Blankenhagen, et. al.), and those imposed at a free surface where the loop shape is lost and the dislocation may be free to move under a more gentile curvature. In the Blanckenhagen, et. al., model the impenetrable boundary sets a new smaller length for the operation of the Frank-Read source, for initial Frank-Read source sizes that are greater than 1/3 the sample dimension. Thus, strengthening of the system occurs as the result of the constrained smaller source length. Herein, single-ended sources form with the dislocation being mobile on the free surface and thus are weaker than the corresponding Frank-Read sources of an equal length in the bulk. However, simulations suggest that microcrystals that form such configurations are strengthened nonetheless.

These findings re-enforce the statistical model suggested by Parthasarathy, et. al., [11] in that the source-strength coefficients are generally of the order of that assumed for the model. Thus, it is readily expected that the single-ended sources can result in hardening a small deforming volume provided that the stochastic aspects of that model are representative of physical microcrystals. In that model it is argued that sources form from an initial dislocation forest of some density and, even though single-ended sources are weaker than the corresponding Frank-Read sources of an identical length, the lengths

of single-ended sources found in microcrystals are, on average, much smaller than Frank-Read sources for a given dislocation density. This is illustrated by Fig. 8 (adapted from [11]) wherein the average length of single-ended sources, scaled by the diameter of the simulation cell, is plotted against the number of initial mobile sources in the sample, again for a fixed starting dislocation density. Also shown in Fig. 8 is the standard deviation in the source lengths as a function of number of initial mobile sources in the sample. Figure 8 clearly shows that as the number of initial mobile sources decreases, the average source length scaled to the diameter decreases significantly. As the number of initial mobile sources decreases (decreasing sample size), the strengths of single-ended sources becomes important, even though they are weaker than equivalent-length double-ended sources. Also as discussed previously, cross-slip induced by image stresses may increase the strengths of single-ended sources to levels that approach those of double-ended sources, thereby making the strength of single-ended sources even more important. Such effects remain to be investigated. Thus, for small micrometer-scale volumes, single-ended sources are expected to control plastic deformation and to lead to high initial stresses in micrometer-sized volumes [11].

In the statistical model of Parthasarathy, et. al., [11] the strength of single-ended sources was taken to be approximately equal to $<\alpha>\mu b/L$, where $<\alpha>$ was taken to be 1. The range of sample diameters considered in the model was 1 – 20 microns and the sample radius was chosen as the maximum source length, L. From that statistical analysis, the average length of single-ended sources, over that range of sample diameters, is a factor of 5 – 10 larger than the value of 933b selected in this study. The simulations presented here give 'α' in the range of 0.54 to 1.12 at a length of 9330b for single-ended

sources and the SSA (equation 4), with an average value of 0.83. Therefore, the value of 1 chosen for $<\alpha>$ in [11] is a slight overestimate of the contribution of source-truncation hardening to the strengthening observed at small sizes in microcrystal experiments [1-8]. However, 3D dislocation dynamics studies [9] show that in addition to source-truncation hardening, another mechanism of strengthening is present in micrometer sized crystals, 'exhaustion hardening', which is related to the cessation of initially-operating single-ended sources due to interaction with obstacles and activation of original source / new source at larger stresses. This second mechanism of strengthening has not been taken into account in the statistical model [11] and could account for discrepancy between the experimental strengthening data and the statistical model of Parthasarathy, et. al.

ACKNOWLEDGEMENT

The authors acknowledge use of the 3D DDS code, ParaDiS, which was developed at Lawrence Livermore National Laboratory by the ParaDiS team. The work of M. Tang is performed under the auspices of the United States Department of Energy by the University of California. This work was supported by the AFOSR, and by a grant of computer time from the DOD High Performance Computing Modernization Program, at the Aeronautical Systems Center/Major Shared Resource Center. The work was performed at the U.S. Air Force Research Laboratory, Materials and Manufacturing Directorate, Wright-Patterson AFB.

REFERENCES

1. Uchic, M. D., Dimiduk, D. M., Florando, J. N. & Nix, W. D., 2003, in: George, E. P., Inui, H., Mills, M.J. & Eggeler, G. editors. *Defect Properties and Related*

Phenomena in Intermetallic Alloys, Materials Research Society Symposium Proceedings, vol. 753. Pittsburgh (PA): Materials Research Society p. 27.

2. Uchic, M. D. & Dimiduk, D. M., 2005, Mater. Sci. Engr. A., **400–401** 268.

3. Dimiduk, D. M., Uchic, M. D. & Parthasarathy ,T. A., 2005, Acta Mater., **53** 4065.

4. Dimiduk, D. M., Woodward, C., LeSar, R. & Uchic, M. D., 2006, Science, **312** 1188.

5. Uchic, M. D., Dimiduk, D. M., Florando, J. N. & Nix, W. D., 2004, Science, **305** 986.

6. Greer, J. R., Oliver, W. C. & Nix, W. D., 2005, Acta Mater., **53** 1821. Errata

7. Volkert, C. A. & Lilliodden, E., 2006, Phil. Mag. **86,** 5567-5579.

8. Dimiduk, D. M., Uchic, M. D., Rao, S. I., Woodward, C. & Parthasarathy, T. A., 2007, Modelling Simul. Mater. Sci. Eng., **15**, 135-146.

9. Rao, S. I., Parthasarathy, T. A., Tang, M., Dimiduk, D.M., Uchic, M.D., & Woodward, C., 2007, to be submitted for publication.

10. Blankenhagen, B. V., Gumbsch, P., & Arzt, E., 2003, Phil.Mag.Letters, **83**, 1.

11. Parthasarathy, T.A., Rao, S.I., Dimiduk, D.M., Uchic, M.D., & Trinkle, D.R., 2007, Scripta. Mater., **56**, 313.

12. Pichaud, B., Minari, F., & Kellerhals, J., 1978, Phil.Mag.A, **38**, 593.

13. Cai W., Bulatov V., Pierce T., Hiratani M., Rhee M., Bartelt M. & Tang M., 2004, Massively-parallel dislocation dynamics simulations in Solid Mechanics and Its applications, edited by Kitagawa, H. & Shibutani, Y. (Kluwer Academic Publishers) **115**, 1.

14. Arsenlis, A., Cai, W., Tang, M., Rhee, M., Oppelstrup, T., Hommes, G., Pierce, T.G., & Bulatov, V.V., 2007, Modelling Simul. Mater.Sci.Eng., accepted for publication.

15. Ardell, A. J., 1985, Metall.Trans. A, **16**, 2131.

16. Bacon, D., Barnett, D., and Scattergood, R., 1978, Prog. Mater. Sci., **23**, 208.

17. Tang M, Cai W, Xu G & Bulatov V, 2006, Modelling Simul. Mater. Sci. Eng., **14**, 1139.

18. Hirth, J. P., & Lothe, J., 1982, Theory of dislocations, second edition, John Wiley and Sons, New York.

19. Hazzledine, P.M., 1985, in Fundamentals of Deformation and Fracture, edited by B.A. Bilby, et al., C.U.P. 385.

20. Tang M, Xu G, Cai W & Bulatov V, 2003, in Thin film stresses and mechanical properties edited by Corocoran S G, Joo Y-C, Moody N R & Zuo Z (Materials Research Society, Warrendale, PA) **U2.4**, 795.

21. Hazzledine, P. M., & Shaibani S. J., 1982, in 6th International Conference on Strength of Metals and Alloys (ICSMA), ed. R.C. Gifkins (Oxford: Pergamon), **1**, 45.

22. Hazzledine, P.M. Karnthaler, H.P. and Wintner, E., 1975, Philos. Mag., **32**, 81-97.

23. Nembach E., 2000, Prog.Mater.Sci., **45**, 275.

24. Madec R., Devincre B., and Kubin L.P., 2002, Phys. Rev. Let., **89**, 255508-1.

FIGURE CAPTIONS

Figure 1: The critical resolved shear stress, $\tau^*(\upsilon)$ for a double-ended source having 30^o mixed dislocation character as a function of Poisson's ratio. Critical stresses are in MPa. The line gives the best fit of the simulation-based empirical relation given by Bacon, et. al., (15) for infinite crystals, with C = 0.823. Results from FFST method are denoted by open symbols.

Figure 2: The critical resolved shear stress, $\tau^*(\upsilon)$ for single-ended source of 30^o mixed character is shown compared with the result for double-ended source of the same length. Critical stresses are in MPa. Unlike the double-ended source, the single-ended source has

a different critical stress depending upon the forward or backward direction of operation. Results from FFST method are denoted by open symbols.

Figure 3: Stress-strain curves for three single-ended sources of length 933b, 30^o forward, 30^o reverse and screw character in a 1 micron cubic cell using the SSA method. Stresses are in MPa. Shear modulus = 59.9 GPa and Poisson's ratio = 0.38. The cubic cell was stressed in the [41-3] direction.

Figure 4: Critical configurations of a 30^o single-ended source moving in the forward and reverse directions and a screw-character source of length 933b in a 1 micron cubic cell. Shear modulus is 59.9 GPa and Poisson's ratio = 0.38. The initial rotation of the 30^o source is also depicted. All results are for the SSA method.

Figure 5: Comparison of the critical configurations of a 30^o single-ended source moving in the forward direction with and without image stresses (both SSA & FFST methods). Shear modulus is 59.9 GPa and Poisson's ratio = 0.38. The initial rotation of the source is also depicted.

Figure 6: The critical resolved shear stresses, $\tau^*(\upsilon)$ for single-ended and double-ended (Frank-Read) sources of 30^o mixed character and length 933b. Results shown are for $\upsilon = 0.1$ and 0.38. Image stresses are included in the simulations using the FFST method. Critical stresses are in MPa.

Figure 7: Critical resolved shear stress (τ^*) of 30^o single-ended and double-ended (Frank-Read) sources as a function of length L of the sources. Also, shown are $k\mu ln(L/b)/(L/b)$ fits to the simulation data (solid lines). $k = 0.06$ (single ended backward); $k = 0.12$ (single ended forward) and $k = 0.18$ (double ended). All results are for the SSA method. Critical stresses are in MPa.

Figure 8: a) Average source length, <L> (scaled to the radius of the sample, R) versus the number of initial mobile sources in the sample (based on an initial dislocation density [11]). b) Schematic illustration of source length probability distributions for microcrystals versus bulk samples following model given in [11].

This work was performed under the auspices of the U. S. Department of Energy by University of California, Lawrence Livermore National Laboratory under Contract W-7405-ENG-48.

Source	α (using SSA)
Single-ended (30^o forward)	0.84
Single-ended (30^o reverse)	0.4
Single-ended (screw)	0.66
Frank-Read (screw)	1.28
Frank-Read (30^o)	1.19
Frank-Read (edge)	0.86

Table 1: Measure of strength of single-ended and Frank-Read sources, 'α', at a Poisson's ratio, υ of 0.38 and length of 933b.

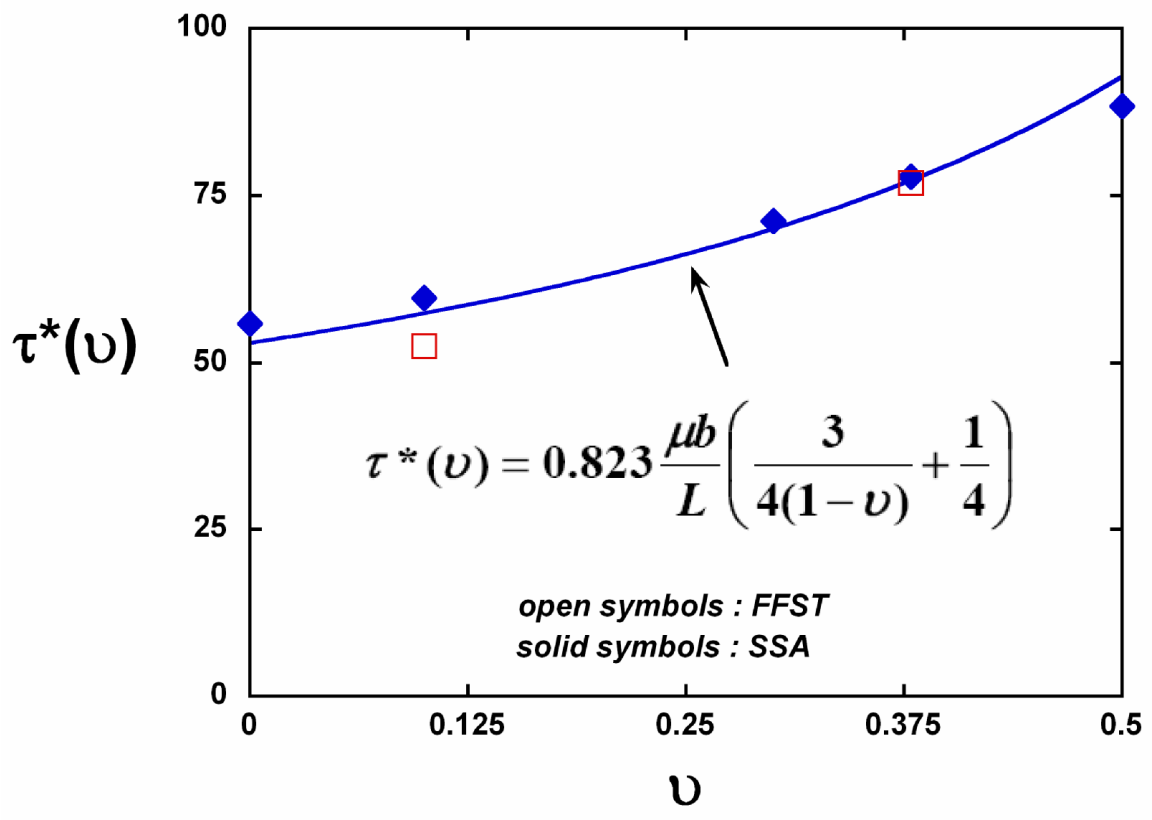

Figure 1: The critical resolved shear stress, $\tau^*(\upsilon)$ for a double-ended source having 30° mixed dislocation character as a function of Poisson's ratio. Critical stresses are in MPa. The line gives the best fit of the simulation-based empirical relation given by Bacon, et. al., (15) for infinite crystals, with C = 0.823. Results from FFST method are denoted by open symbols.

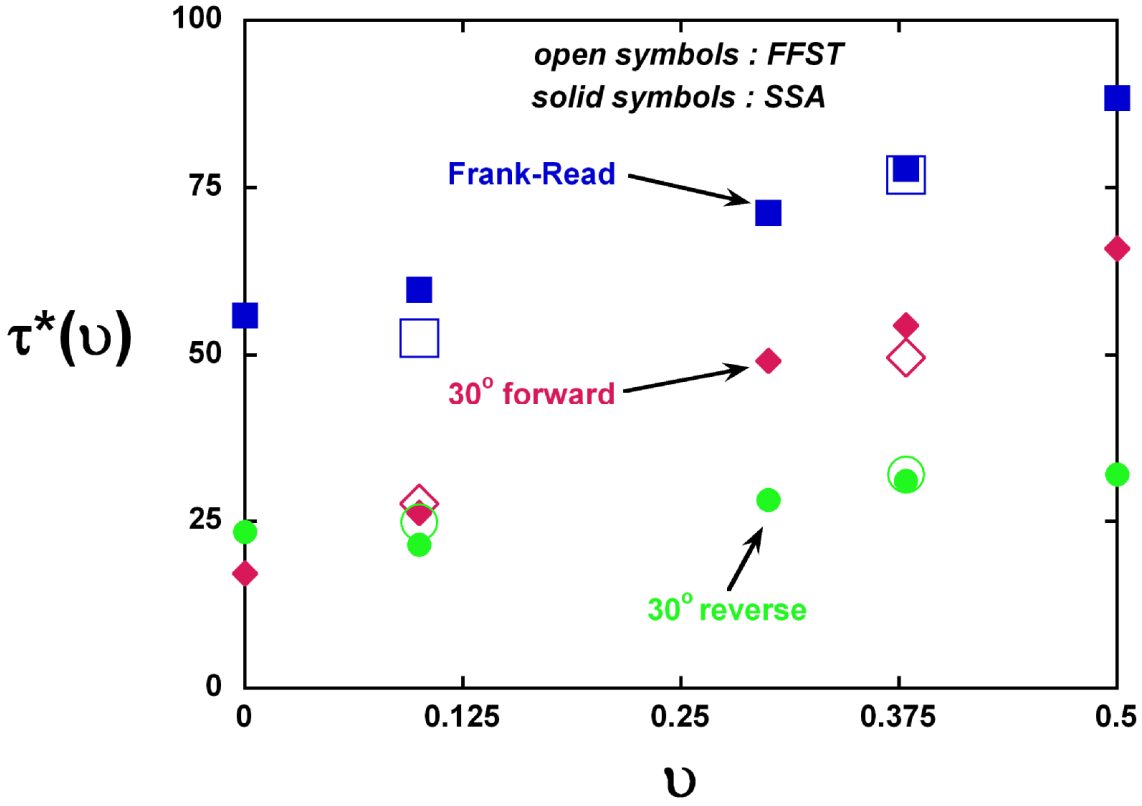

Figure 2: The critical resolved shear stress, $\tau^*(\upsilon)$ for single-ended source of 30^o mixed character is shown compared with the result for double-ended source of the same length. Critical stresses are in MPa. Unlike the double-ended source, the single-ended source has a different critical stress depending upon the forward or backward direction of operation. Results FFST method are denoted by open symbols.

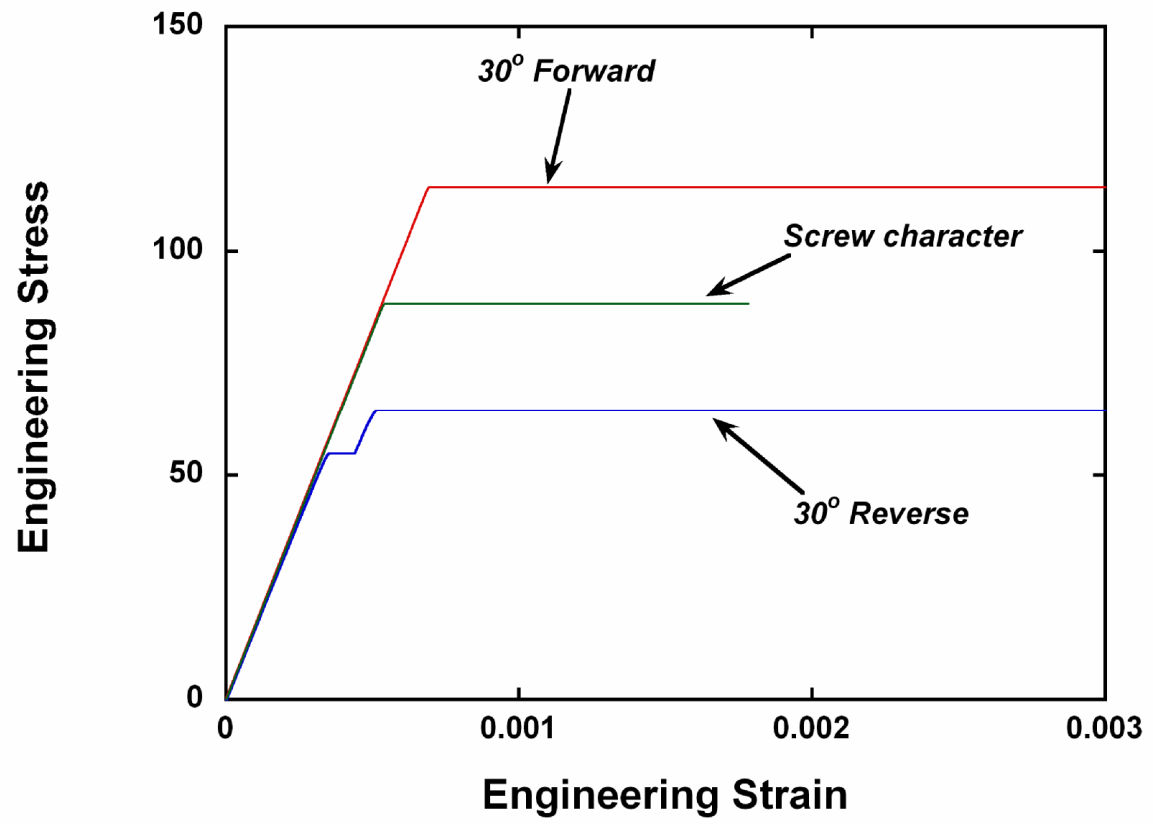

Figure 3: Stress-strain curves for three single-ended sources of length 933b, 30° forward, 30° reverse and screw character in a 1 micron cubic cell using the SSA method. Stresses are in MPa. Shear modulus = 59.9 GPa and Poisson's ratio = 0.38. The cubic cell was stressed in the [41-3] direction.

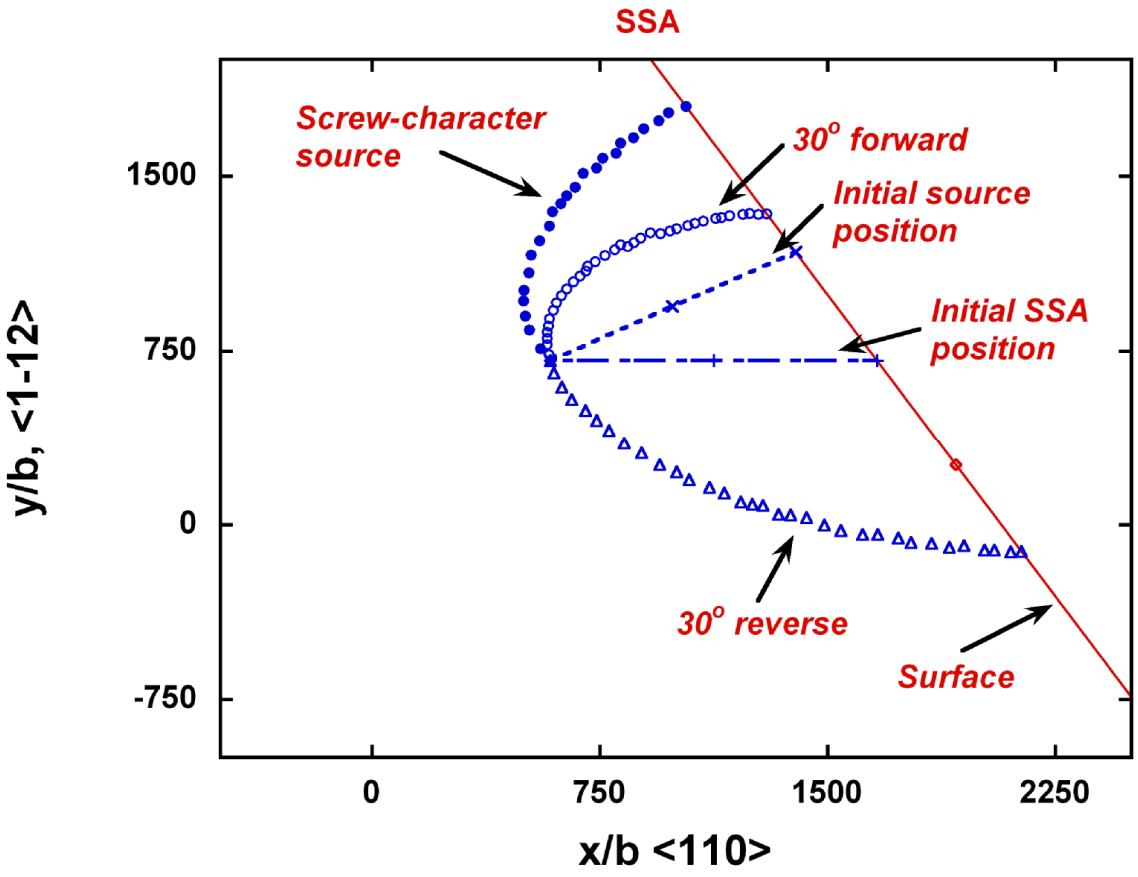

Figure 4: Critical configurations of a 30° single-ended source moving in the forward and reverse directions and a screw-character source of length 933b in a 1 micron cubic cell. Shear modulus is 59.9 GPa and Poisson's ratio = 0.38. The initial rotation of the 30° source is also depicted. All results are for the SSA method.

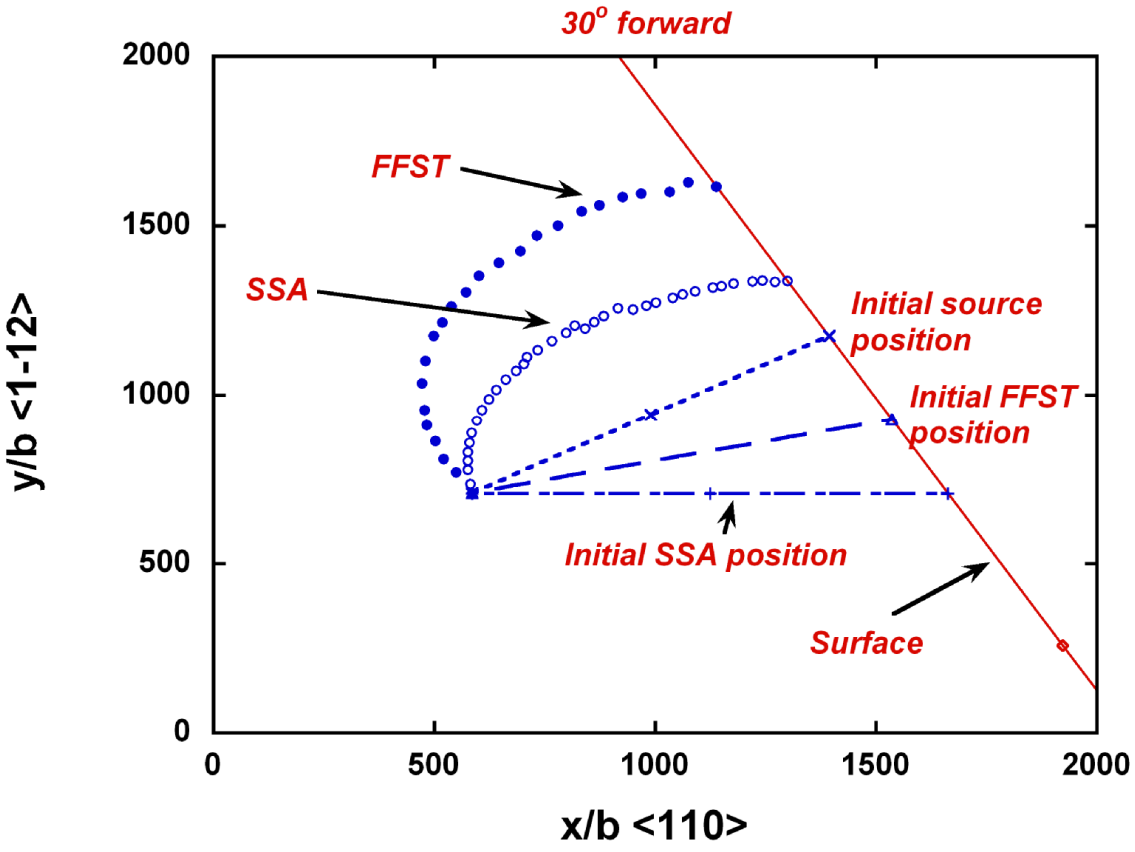

Figure 5: Comparison of the critical configurations of a 30° single-ended source moving in the forward direction with and without image stresses (both SSA & FFST methods). Shear modulus is 59.9 GPa and Poisson's ratio = 0.38. The initial rotation of the source is also depicted.

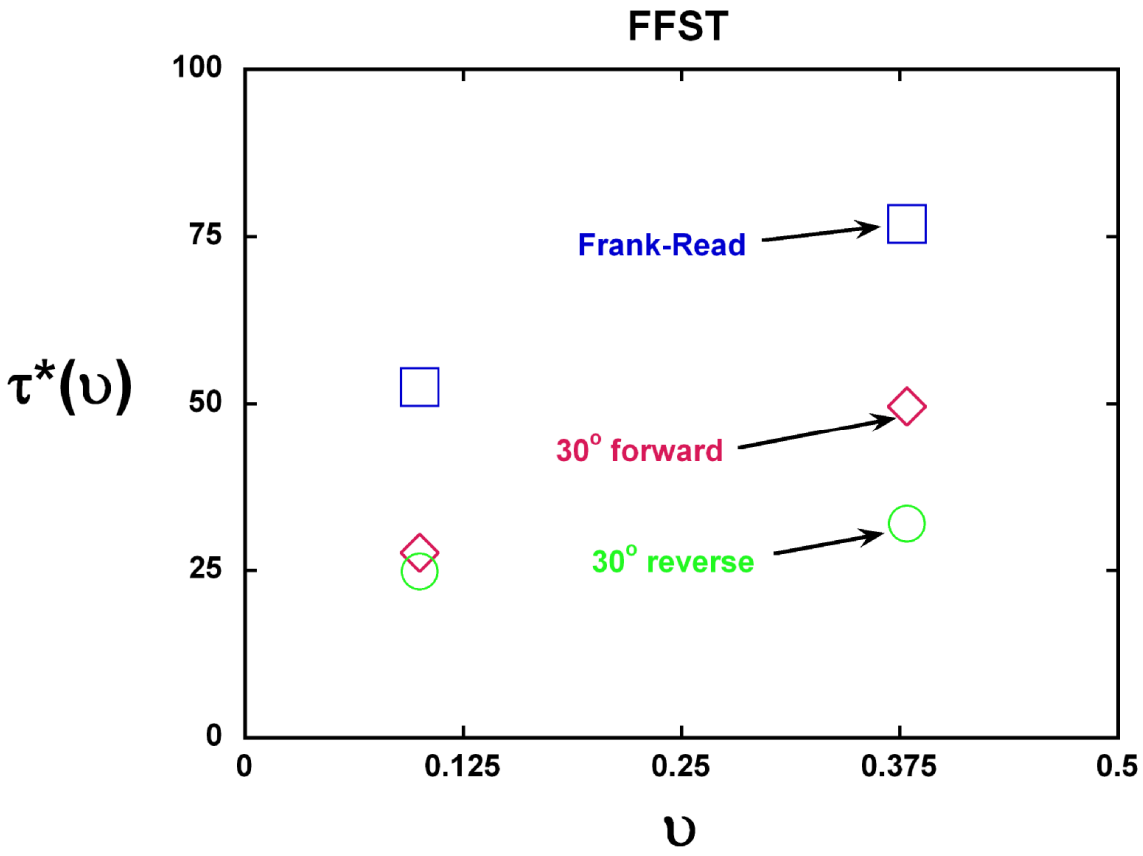

Figure 6: The critical resolved shear stresses, $\tau^*(\upsilon)$ for single-ended and double-ended (Frank-Read) sources of 30° mixed character and length 933b. Results shown are for $\upsilon = 0.1$ and 0.38. Image stresses are included in the simulations using the FFST method. Critical stresses are in MPa.

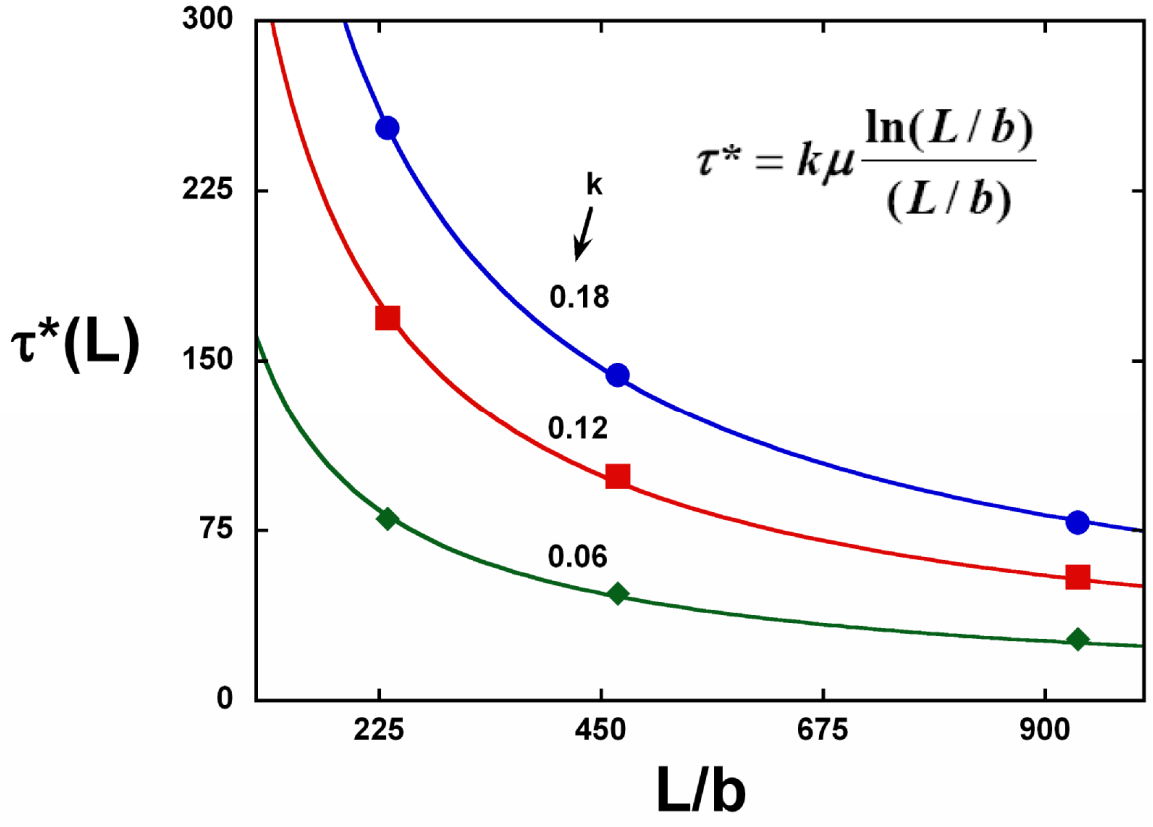

Figure 7: Critical resolved shear stress (τ*) of 30° single-ended and double-ended (Frank-Read) sources as a function of length L of the sources. Also, shown are kμln(L/b)/(L/b) fits to the simulation data (solid lines). k = 0.06 (single ended backward); k = 0.12 (single ended forward) and k = 0.18 (double ended). All results are for the SSA method. Critical stresses are in MPa.

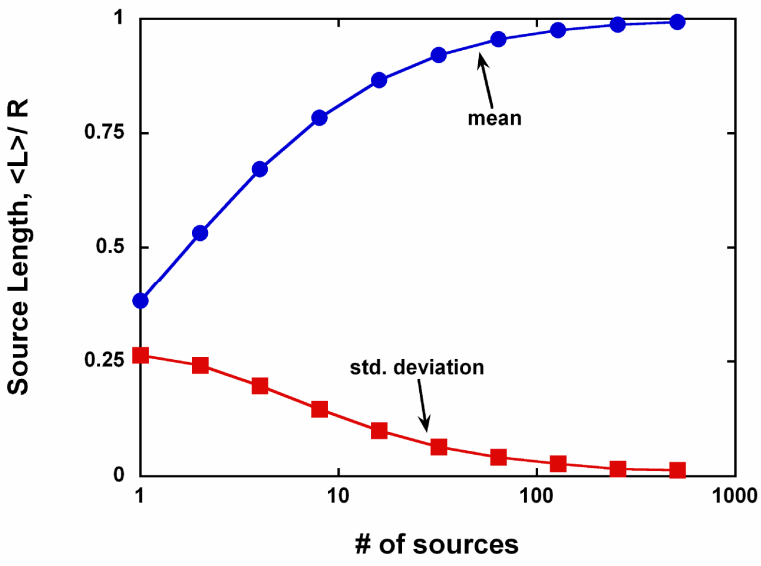

(a)

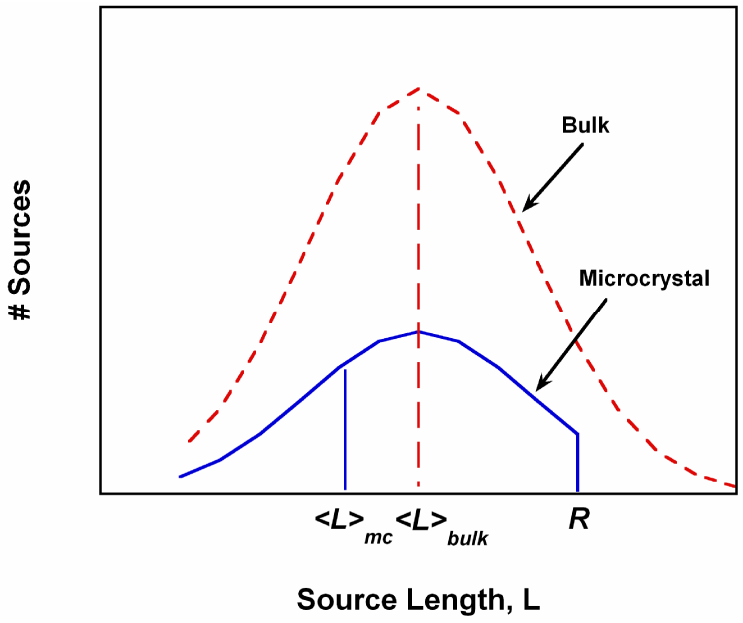

(b)

Figure 8: a) Average source length, <L>, as well as the standard deviation in <L> (scaled to the radius of the sample, R) versus the number of initial mobile sources in the sample (based on an initial dislocation density [11]). b) Schematic illustration of source length distributions for microcrystals versus bulk samples following model given in [11].